Journal of Advanced Research 9 (2018) 27–33

Contents lists available at ScienceDirect

Journal of Advanced Research

journal homepage: www.elsevier.com/locate/jare

Original Article

Electronic and magnetic properties of the [Ni(salophen)]: An experimental and DFT study

Rodrigo A. Mendes [a], José Carlos Germino [b], Bruno R. Fazolo [a], Ericson H.N.S. Thaines [a], Franklin Ferraro [c], Anderson M. Santana [a], Romildo J. Ramos [a], Gabriel L.C. de Souza [a], Renato G. Freitas [a], Pedro A.M. Vazquez [b], Cristina A. Barboza [d,*]

[a] LCM – Laboratório Computacional de Materiais – Department of Chemistry, Federal University of Mato Grosso–UFMT, Cuiabá, Brazil
[b] Chemistry Institute, State University of Campinas – UNICAMP, Campinas, Brazil
[c] Departamento de Ciencias Básicas, Universidad Católica Luis Amigó, Medellin, Colombia
[d] Institute of Physics, Polish Academy of Sciences, 02 668 Warsaw, Poland

GRAPHICAL ABSTRACT

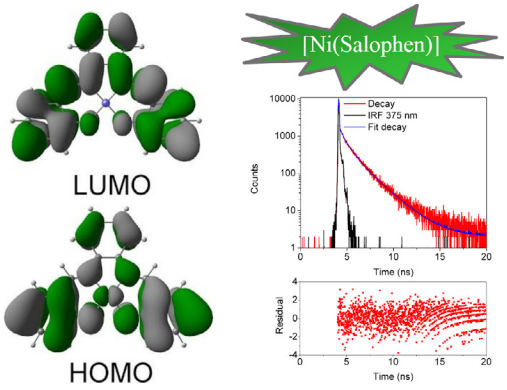

ARTICLE INFO

Article history:
Received 11 August 2017
Revised 14 October 2017
Accepted 16 October 2017
Available online 16 October 2017

Keywords:
Salophen
Nickel complex
Photoluminescence
TD-DFT
NTO
Magnetically induced rings

ABSTRACT

The effect of the coordination of a Ni(II) ion on the electronic and magnetic properties of the ligand salophen were experimentally and theoretically evaluated. The complex [Ni(salophen)] was synthesized and characterized through FTIR and an elemental analysis. Spectral data obtained using DMSO as a solvent showed that the ligand absorption profile was significantly disturbed after the coordination of the metal atom. In addition to a redshift of the salophen ligand absorption bands, mainly composed by $\pi \rightarrow \pi^*$electronic transitions, additional bands of around 470 nm were observed, resulting in a partial metal-to-ligand charge transfer. Furthermore, a significant increment of its band intensities was observed, favoring a more intense absorption in a broader range of the visible spectrum, which is a desired characteristic for applications in the field of organic electronics. This finding is related to an increment of the planarity and consequent electron delocalization of the macrocycle in the complex, which was estimated by the calculation of the current strengths at the PBE0/cc-pVTZ (Dyall.v3z for Ni(II)) level.

Introduction

Recently, there has been an increased interest in the chemistry of transition metal complexes containing N_2O_2 coordination sites,

Peer review under responsibility of Cairo University.
* Corresponding author.
E-mail address: crissetubal@ifpan.edu.pl (C.A. Barboza).

https://doi.org/10.1016/j.jare.2017.10.004
2090-1232/

such as salicylidenes [1], due to their broad range of applications in areas such as catalysis [2], functional materials, non-linear optics [3], molecular magnetism [4], and organic electronics [5], such as light emitting diodes (OLEDs) [6] and display magnetic properties [7]. Among them, technologies based on light emission or charge transport abilities are currently receiving particular interest, leading to their use in electronic devices, such as solar cells and active components for image and data treatment storage [8]. Salicylidenes are a type of Schiff base derived from the condensation of a primary amine with a salicylaldehyde derivative. Numerous substituents can be placed on the phenol ring, and the imine bridge allows for tuning the size and the shape of the complexes to control their self-assembly on surfaces [9]. A schematic structure can be observed in Fig. 1.

Their easiness along with the synthesis and modulation of the physical-chemical properties of salicylidenes make them a versatile and interesting class of molecules [1,10]. Their molecular structure and capable coordinate sites make salicylidenes flexible coordination compounds with several metal ions, such as Ni(II), Cu(II), Zn(II), Ru(II), Os(II), Pt(II), and Ir(III) [3]. A variety of metal ions (diamagnetic and paramagnetic) can be introduced in the coordination site, in most cases forming square planar array frameworks [6]. Schiff base nickel(II) salen-type complexes have been extensively used in catalysis [7,9] and for biological purposes [11].

Salophen metal complexes are planar systems composed of three aromatic rings [12]. Aromatic molecules are known for their ability to sustain diatropic currents when exposed to an external magnetic field. For instance, when applying a perpendicular magnetic field towards the plane of the aromatic system, a ring current is induced along the delocalized π electrons [13]. The strength and the pathway of the magnetically induced current flow sustained by delocalized electrons in molecular systems play an important role in nanotechnological applications, such as molecular switches or optical devices [13]. The current pathways and the flow along chemical bonds and around molecular rings reflect the electron delocalization in macrocycles, such as porphyrins and fullerenes [14]. Several methodologies are used to calculate magnetically induced current strengths [15]; however, to evaluate the effect of the modification of the central metal atom on the electronic delocalization of the salophen framework, the magnetically induced current method [16] proposed by Sulzer et al. [17] was chosen for this study.

To investigate the potential use of these compounds for optical devices such as solar cells, structural, electronic, and magnetic properties were calculated at the DFT/TD-DFT level, which has been proven useful in evaluating the electronic structure of this type of complex [7,18]. The obtained results were correlated with the experimental measurements.

Material and methods

All solvents and reagents were used as purchased from Sigma-Aldrich (São Paulo, São Paulo, Brazil) without further purification. The infrared spectra of KBr pellets of the complex were obtained and measured with a Varian 600-IR spectrometer (Atibaia, São Paulo, Brazil). The TG/DTA curves were obtained in a Shimadzu apparatus (Kyoto, Japan) with a heating rate of 10 °C cm^{-1} using a dynamic atmosphere of synthetic air at a flow rate of 100 mL min^{-1} until 800 °C. The crystal structure of the salophen ligand has been reported [6]. The electronic absorption spectra of salophen and [Ni(salophen)] in DMSO solutions (1×10^{-5} mol L^{-1}) were acquired using a Hewlett-Packard 8452A diode array UV−vis spectrophotometer (Santa Clara, California, United States). The steady-state fluorescence spectrum was acquired using an ISS PC1 spectrofluorometer (Champaign, Illinois, United States) of λ_{exc} = 378 nm in a 1.0 cm quartz cuvette (model 111-10-40, type 111-QS, Hellma Analytics, Plainview, New York, United States).

Fluorescence decay was recorded using time-correlated single photon counting and an Edinburgh Analytical Instruments FL 900 spectrofluorimeter (Livingston, Scotland) with an MCP-PMT detector (Hamamatsu R3809U-50). The excitation wavelength for [Ni(salophen)] in the DMSO solution was λ_{exc} = 375 nm (Edinburgh model EPL-375, Livingston, Scotland, with a 10 nm bandwidth, 77.0 ps). The decay signals for this sample were collected at λ_{PL} = 420 nm. The instrument response was recorded using Ludox samples. At least 10,000 counts in the peak channel were accumulated for the lifetime measurements. The emission decays were analyzed using exponential functions.

Synthesis

The procedure to obtain the ligand (salophen) has been described in detail [6]. [Ni(salophen)] was obtained by dissolving the salophen ligand (158 mg; 0.5 mmol) in ethanol (20 mL) after stirring until total solubility on a round flask balloon. Then, an ethanolic solution of NaOH (40 mg; 1.0 mmol) was slowly dropped into the reaction system. After 5 min, $NiSO_4$ (77.5 mg; 0.5 mmol) was added to the mixture, and a [Ni(salophen)] coordination complex instantly formed. As a result, a polycrystaline deep-red powder was obtained with a 67% yield. The main infrared bands measured in the KBr pellet were ν_{Ni-O} = 457, ν_{Ni-N} = 545, ν_{C-N} = 1610, ν_{C-O} = 1197, ν_{C-H} = 3050, and ν_{Ar} = 755 (cm^{-1}) (Fig. S1). The TGA experimental weight loss (wt%, in parenthesis calculated values) was: 47.84 (47.76) (280–468 °C) and 32.15 (32.22) (468–510 °C) ligand pyrolysis and residual 20.01 (20.02) – NiO (Fig. S2). X-ray diffraction residual characterization was performed

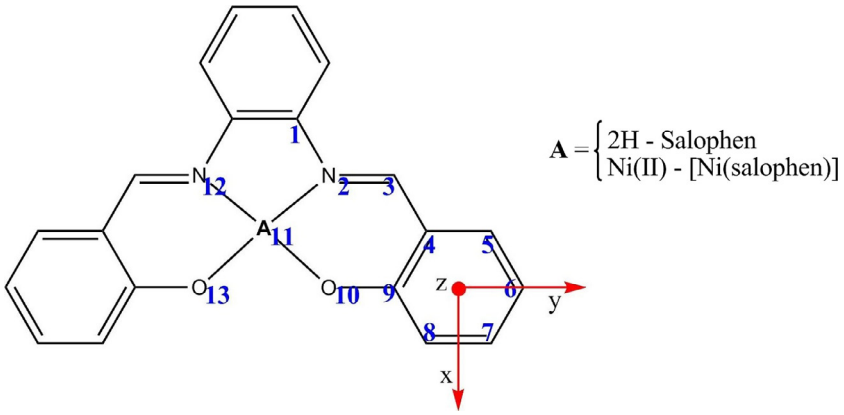

Fig. 1. Molecular structures of the salophen and its Ni(II) coordination compound with principal atom labels and the position of the Cartesian axes.

according to the X-ray Data Bank files with PDF number 01-071-1179 (Tune Cell) NiO-Bunsenite (Fig. S3).

Computational details

The calculations were performed within the density functional theory and its time-dependent counterpart (DFT and TD-DFT). This level of calculation has yielded reliable results in predicting the electronic spectra of chromospheres at a relatively low computational cost, and it is one of the most popular methods used for the evaluation of excitation energies [6,12]. The ground and first active singlet state structures of [Ni(salophen)] were optimized at the PBE0/6-311++G(d,p) [19–21] level of the theory using Gaussian 09 [22]. Vertical excitation energies for 30 low-lying excited states were calculated. To determine the solvent effect (DMSO, $\varepsilon = 46.826$), the polarizable continuum method - PCM approximation was used, defining the cavity unit as a universal forcefield – UFF, and the cavity type scaled the van der Wall surface ($\alpha = 1.10$ 0) [23,24].

The magnetically induced current density maps were evaluated with DIRAC [25] software using the four component relativistic Dirac-Coulomb Hamiltonian [26]. These results were obtained using perturbation-dependent basis sets that shift the gauge origin to their respective center, thereby ensuring that the calculated magnetic properties are independent of the position of the gauge origin [27]. For the large component, triple-ζ quality Dyall basis sets for the nickel(II) atom was used, while for the light atoms, an uncontracted Dunning cc-pVTZ basis set was chosen [28]. The induced current density streamline plots were visualized using the PyNGL package [29]. The integration plane was chosen to be perpendicular to the molecular plane, beginning from the center of mass and extending to 10 atomic units in all directions. This plane cuts a C—C bond and allows for obtaining the net current intensity around the molecular framework.

Results and discussion

Molecular structures

The salophen and [Ni(salophen)] ground (S_0) and first active excited state (S_1) structures were optimized at the PBE0/6-311++G(d,p) level. The research group observed the remarkable quality of the PBE0 functional results in a previous paper for [Zn(salophen)(OH_2)] [6] optimization compared to crystal structures obtained by Rietveld refinement. Also, according to Barone et al. [30], PBE0 functional results are slightly more reliable than B3LYP for a set of small organic molecules. The respective structures and main bond lengths are provided in Table S1. As previously noted for [Zn(salophen)(OH_2)], the coordination of the nickel(II) ion to the ligand leads to a significant increment in the ligand planarity. Respective to the S_0 and S_1 structures of the complex, there was no significant difference due to the rigidity of the structures; however, the structure corresponding to the first active singlet S_1 of the ligand had a higher symmetry (corresponding to the point group C_2) and was more planar than the ground state.

Similar bond lengths were observed in the literature for [M(salophen)] (M = Mn, Ni, Cu, and Zn) and related molecular structures [31,32]. For [Zn(salophen)(OH_2)], the coordination site bond distances calculated at the PBE0/6-311G++(d,p) level are equal to 2.104 and 1.987 Å for M-N_{12} and M-O_{10}, respectively. For [Ni(salophen)] obtained using B3LYP/6-31G(d), these values are 1.860 and 1.842 Å, respectively, which is in agreement with crystal refinement obtained by Lecarme et al. [32], who also studied the electronic structure of [Ni(salophen)]-related structures, focusing on one-electron-oxidized Ni(II) salophen complex and its amino derivatives. Optimized structures obtained for [Cu(salophen)] and [Ni(salophen)] at the PBE0/def-TZVP level reported by Zarei et al. [31] showed the bond lengths to be: 1.959 and 1.910 and 1.881 and 1.853 Å for Cu—N_{12}, Cu—O_{10}, Ni—N_{12}, and Ni—O_{10}, respectively. Finally, Atakol et al. [33] identified the structural positions of [Ni(salophen)]-related molecular structures via crystal refinement using the DRX technique. The same value for Ni—N_{12} bond length 1.867 Å was also obtained as herein reported.

Steady-State absorption spectra and calculated electronic transitions

Salophen and [Ni(salophen)] absorption spectra were measured in a DMSO solution (1×10^{-5} mol L^{-1}), and the data obtained are presented in Table 1 and Fig. 2. Salophen electronic absorption spectra in a DMSO solution were reported in a previous work [6] to exhibit two absorption bands centered at 270 and 335 nm ($\varepsilon = 2.08$ and 1.48×10^4 L mol^{-1} cm^{-1}, respectively) assigned to $\pi \rightarrow \pi*$ electronic transitions, mainly involving the frontier orbitals spread over the ligand structure. Due to the increment of the electron delocalization of the macrocycle in the complex, the ligand absorption bands were redshifted to 302 and 378 nm ($\varepsilon = 1.69$ and 2.67×10^4 L mol^{-1} cm^{-1}, respectively). In addition, a band was observed at 478 nm ($\varepsilon = 8.42 \times 10^3$ L mol^{-1} cm^{-1}) due to the

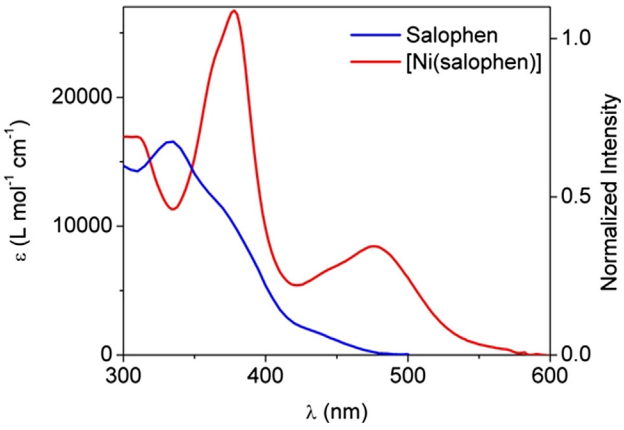

Fig. 2. Electronic absorption of the salophen ligand (blue) and [Ni(salophen)] coordination compound (red) measured in DMSO (1×10^{-5} mol L^{-1}).

Table 1
Excitation energies experimentally obtained and calculated at the PBE0/6-311++G(d,p) level for [Ni(salophen)] using DMSO as solvent.

	λ_{exptl}/nm	E/eV	λ/nm	*f*	Assignment[a]
Salophen	370	3.28	378	0.46	100% H → L
	335	3.71	334	0.80	60% H-1 → L; 40% H → L+1
[Ni(salophen)]	478	2.80	442	0.28	100% H-1 → L
	378	3.36	369	0.55	100% H-1 → L+1
	302	3.61	344	0.69	100% H-2 → L

[a] H = HOMO and L = LUMO.

contribution of the atomic orbitals *d* of the Ni(II) ion to the frontier molecular orbitals involved in the electronic transitions.

To obtain more information regarding the nature of these excitations, theoretical calculations were performed using a PBE0/6-311++G(d,p) basis set and DMSO as a solvent according to the PCM approach. As can be seen in the energy diagram given in Fig. 3, frontier molecular orbitals are degenerate; hence, all electronic transitions are mainly located in the ligand of a $\pi \rightarrow \pi*$ type, which involves molecular orbitals mainly located over the ligand framework. There is also a contribution of the metal atom to the complex transitions, resulting in a partial metal-to-ligand charge transfer (^{1}ILCT/^{1}MLCT), favoring the destabilization of the frontier molecular orbitals and resulting in a redshift of the absorption bands respective to the free basis ligand. Despite the larger deviation of the excitation energies of the complex from the experimental data, the results are still within the expected accuracy of TD-DFT using hybrid density functionals of around 0.3 eV [37]. It has been pointed out that TDDFT also yields substantial errors for excited states of molecules with extended π-systems [38,39] as well for charge-transfer (CT) states [40,41], as observed for the complex [Ni(salophen)]. Lecarme et al. [32] also observed a similar deviation for [Ni(salophen)], where CT could be observed. According to Jacquemin et al. [37], a deviation in a TDDFT calculation can be related to a long-range charge transfer, a potential energy surface, non-Franck-Condon transitions, or a singlet-triplet transition. Although a small deviation of the excitation energies of the complex from the experimental data was observed, a diffuse orbitals base set (mandatory for CT states) and a global hybrid functional PBE0 were responsible for decreasing the deviation. Despite these failures of TDDFT, it has been applied to large molecular systems [42] in which inter- or intra-molecular CT states might play important roles.

Photoluminescence spectra

Fig. 4 presents the steady-state photoluminescence (PL) spectrum of [Ni(salophen)] obtained in DMSO (λ_{exc} = 378 nm; 1×10^{-5} mol L^{-1}) with only one emission band at the blue-region centered at λ_{PL} = 420 nm with a Stokes Shift respective to the excitation wavelength of *SS* = 2646 cm^{-1}.

As observed by Nijegorodov et al. [1], for a series of planar and non-planar molecules, due to the increment of the rigidity of the ligand after the coordination of the metal atom, the Stokes shift for [Ni(salophen)] is significantly lower (~6000 cm^{-1}) than the free basis ligand reported in Ref. [5]. Hence, the complex emission band appears at a lower wavelength than its free basis ligand. Its fluorescence decay (λ_{exc} = 375 nm; λ_{PL} = 420 nm) was also measured (Fig. 5). A biexponential decay profile was observed, presenting two fluorescence lifetimes: a shorter lifetime of τ_1 = 0.815 ± 0.025 ns (41%) and a longer lifetime of τ_2 = 1.958 ± 0.037 ns (59%). Thus, the two fluorescence lifetimes were attributed to the same chromophore group but with different solvent environments.

According to Atvars et al. [6], a faster decay indicates that the metal disturbs the electronic excited states of the ligand, which

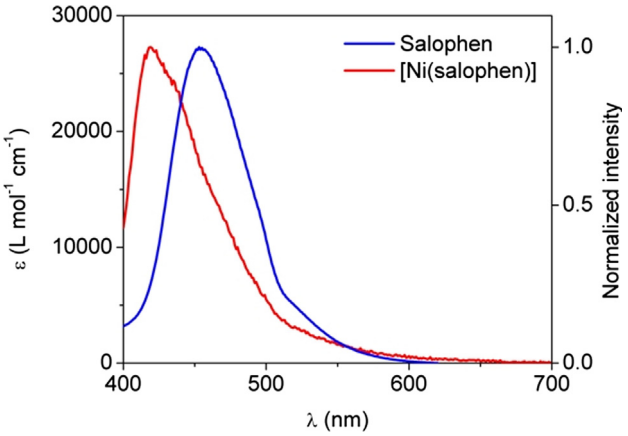

Fig. 4. Steady-state photoluminescence spectrum of the salophen ligand (blue) and [Ni(salophen)] coordination compound (red) measured in DMSO (1×10^{-5} mol L^{-1}).

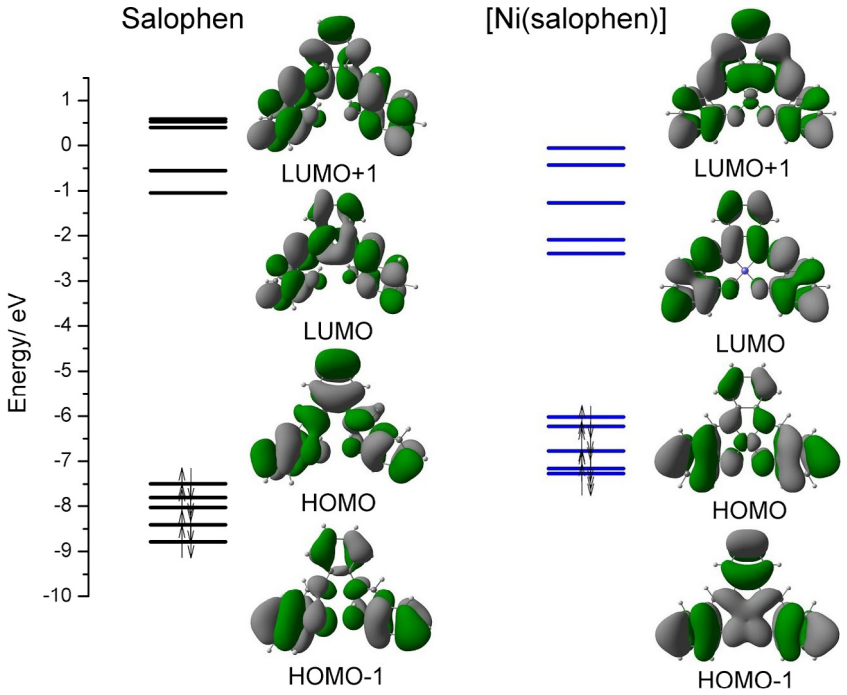

Fig. 3. Frontier molecular orbital energy diagram for salophen and [Ni(salophen)] obtained at PBE0/6-311++G(d,p).

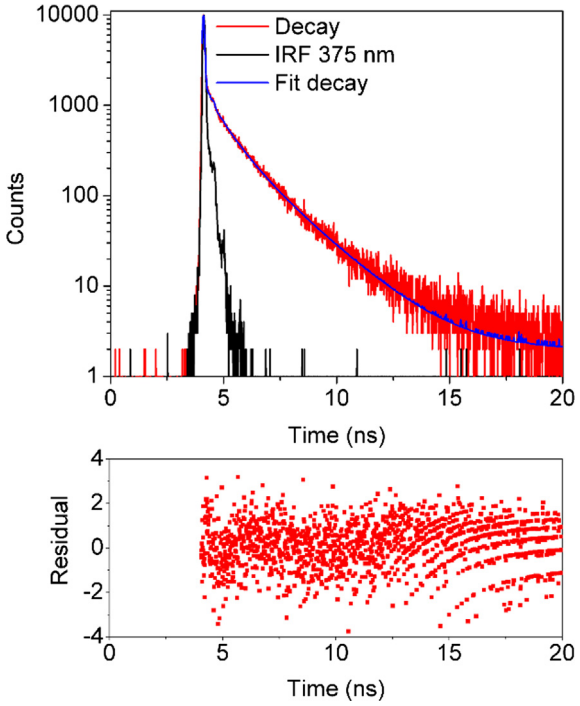

Fig. 5. Fluorescence decays of [Ni(salophen)] measured in DMSO.

is in agreement with the observations of Chavan et al. [34]. For related complexes, the emission observed for [Ni(salophen)] predominantly originated not only due to the $\pi \rightarrow \pi^*$ intra ligand transition but also due to specific MLCT characteristics. This behavior was also observed for Zn(II) salicylidenes in solutions and solid states [35] but with different contributions of the fluorescence lifetimes. Its Ni(II) complex does not present phosphorescence emissions at room temperature in a DMSO solution.

Magnetically induced currents

To evaluate the impact of the nickel(II) atom coordination modification on the electronic delocalization of the salophen ligand, magnetically induced currents were calculated at the PBE0/cc-pVTZ (dyall.v3z for the nickel atom) level, and the results are shown in Fig. 6. According to the chosen methodology, the total probability current density can be separated into paratropic (counter-clockwise) and diatropic (clockwise) components when a magnetic field is perpendicularly directed to the plane of the aromatic system. Located at 1 Å over the molecular plane to mainly consider the contribution from the π orbitals of the aromatic ring, a diatropic probability current can be observed outside the carbon atoms of the ligand framework, and an opposite paratropic current inside the carbon rings is visible for both molecules. It was observed that for both salophen and the [Ni(salophen)] complex, the diatropic ring current π system dominates the streamline plot.

Table 2
Diatropic and paratropic contributions to the net ring current strength (in nA T^{-1}) for salophen and [Ni(salophen)]. The currents are obtained at the PBE0/cc-pVTZ (dyall.v3z for the nickel(II)) level.

	Diatropic	Paratropic	Total
Salophen	101.77	−92.39	9.38
[Ni(salophen)]	110.57	−103.14	7.43

A quantitative analysis of the strength of the magnetically induced ring was performed using the numerical integration of the current density passing a C—C bond from the phenolic ring perpendicular to the XZ plane, as shown in Fig. 1. The total integrated ring current susceptibilities along with their paramagnetic and diamagnetic contributions are presented in Table 2.

According to these results, both molecules have a net ring current of the same order as benzene (~12 nA T^{-1}) [36]. Also, Sundholm et al. [43] studied magnetically induced current density susceptibility along Zn(II)-octaethylporphyrin. According to the authors, at the pyrrole rings, the magnetically induced current values were the same order (by ~11.9 nA T^{-1}). Although there was a larger value of the total integrated magnetically induced current values for the salophen and [Ni(salophen)] complex, the diamagnetic current was stronger (by ~10 nA T^{-1}) for the complex than for the ligand due to the planarization of the ligand framework caused by the coordination of the nickel(II) ion. These findings support the changes observed in the ligand absorption spectra that occur after metal coordination.

Conclusions

In this article, the electronic and magnetic properties of [Ni(salophen)] and the effect of the nickel(II) coordination on the ligand characteristics were theoretically and experimentally evaluated. The spectral data obtained was measured in DMSO and showed a

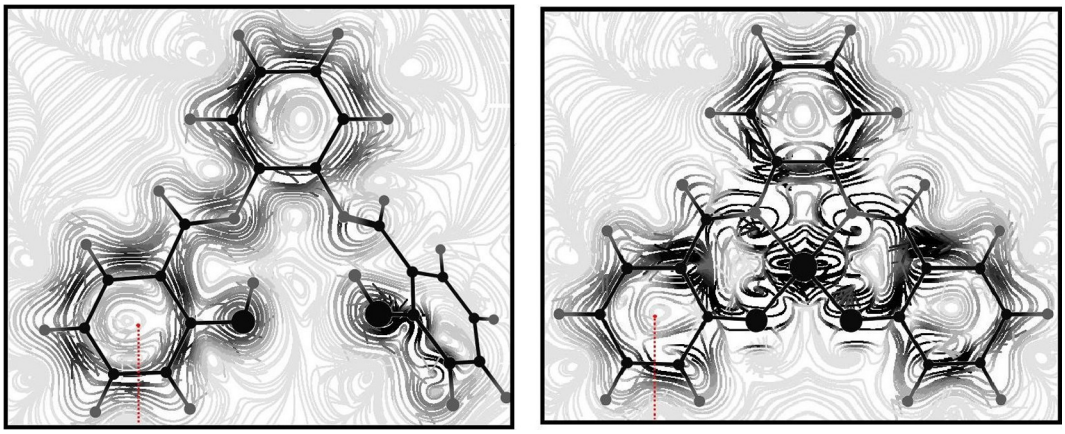

Fig. 6. Induced total probability current density salophen and [Ni(salophen)], obtained 1 Å over the molecular plane at the PBE0/cc-pVTZ (Dyall.v3z for Ni(II)) level. The magnetic field vector points towards the reader. Line intensity is proportional to the norm of the probability current density vector. The atomic centers are represented by dots, and the position of the integration plane is indicated by a red dotted line.

red shift of the ligand absorption bands, mainly composed by $\pi \rightarrow \pi^*$ electronic transitions, after the coordination of the nickel(II) ion. In addition, there was a contribution of d metal orbitals to the complex transitions, resulting in a partial metal-to-ligand charge transfer, which caused the appearance of a low-lying absorption band of around 470 nm. Furthermore, a significant increment of its band intensities was observed, favoring absorption in a broader range of the visible spectrum, a desired characteristic for applications in organic electronics, such as solar cells. This finding is related to the increment of the planarity and the consequent electron delocalization of the macrocycle in the complex, which was estimated using the calculations of the current strengths.

Conflict of interest

The authors have declared no conflict of interest.

Compliance with Ethics Requirements

This article does not contain any studies with human or animal subjects.

Acknowledgements

This research was suported by the Fundação de Amparo à Pesquisa do Estado de São Paulo (FAPESP-grant 2013/16245-2), Fundação de Amparo à Pesquisa do Estado de Mato Grosso (FAPEMAT-grant 214599/2015), Conselho Nacional de Desenvolvimento Científico e Tecnológico (CNPq), Coordenação de Aperfeiçoamento de Pessoal de Nível Superior (CAPES), and the National Institute of Organic Electronics (INEO) (MCT/CNPq/FAPESP), UNICAMP/FAEPEX. The authors would like to thank professors Teresa D.Z. Atvars (UNICAMP), Rogerio J. Prado (UFMT), Ailton J. Terezo (UFMT), and Adriano Buzzuti (UFMT). This research was supported in part by PLGrid infrastructure, and we are also grateful to GRID/UNESP, LCCA/USP, and CENAPAD/SP (Proj650) for providing the computational time.

Appendix A. Supplementary material

Supplementary data associated with this article can be found, in the online version, at https://doi.org/10.1016/j.jare.2017.10.004.

References

[1] Nijegorodov N, Luhanga P, Nkoma J, Winkoun D. The influence of planarity, rigidity and internal heavy atom upon fluorescence parameters and the intersystem crossing rate constant in molecules with the biphenyl basis. Spectrochim Acta A Mol Biomol Spectrosc 2006;64(1):1–5.
[2] Gaur A, Shrivastava BD, Srivastava K, Prasad J, Singh SK. XAFS investigations of copper(II) complexes with tetradentate Schiff base ligands. X-ray Spectrom 2012;41(6):384–92.
[3] Di Bella S, Oliveri IP, Colombo A, Dragonetti C, Righetto S, Roberto D. An unprecedented switching of the second-order nonlinear optical response in aggregate bis (salicylaldiminato) zinc (II) Schiff-base complexes. Dalton Trans 2012;41(23):7013–6.
[4] Andres H, Basler R, Blake AJ, Cadiou C, Chaboussant G, Grant CM, et al. Studies of a nickel-based single-molecule magnet. Chem Eur J 2002;8(21):4867–76.
[5] Staykov A, Watanabe M, Ishihara T, Yoshizawa K. Photoswitching of conductance through salicylidene methylamine. J Phys Chem C 2014;118 (47):27539–48.
[6] Barboza CA, Germino JC, Santana AM, Quites FJ, Vazquez PAM, Atvars TDZ. Structural correlations between luminescent properties and excited state internal proton transfer in some Zinc(II) N,N′-Bis(salicylidenes). J Phys Chem C 2015;119(11):6152–63.
[7] Takjoo R, Akbari A, Ebrahimipour SY, Rrudbari HA, Brunò G. Synthesis, characterization, X-ray structure and DFT calculation of two Mo (VI) and Ni (II) Schiff-base complexes. C R Chim 2014;17(11):1144–53.
[8] Bhattacharjee CR, Datta C, Das G, Chakrabarty R, Mondal P. Induction of photoluminescence and columnar mesomorphism in hemi-disc salphen type Schiff bases via nickel (II) coordination. Polyhedron 2012;33(1):417–24.
[9] Wang Q, Liu Y, Gao W, Xu Z, Li Y, Li W, et al. Transformation of a ditopic Schiff base nickel (II) nitrate complex into an unsymmetrical Schiff base complex by partial hydrolytic degradation: structural and density functional theory studies. Transit Met Chem 2014;39(6):613–21.
[10] Novoa N, Roisnel T, Hamon P, Kahlal S, Manzur C, Ngo HM, et al. Four-coordinate nickel (II) and copper (II) complex based ONO tridentate Schiff base ligands: synthesis, molecular structure, electrochemical, linear and nonlinear properties, and computational study. Dalton Trans 2015;44(41):18019–37.
[11] Dhanaraj CJ, Johnson J. Spectral, thermal, electrochemical, biological and DFT studies on nanocrystalline Co (II), Ni (II), Cu (II) and Zn (II) complexes with a tridentate ONO donor Schiff base ligand. J Coord Chem 2015;68(14):2449–69.
[12] Vivas MG, Germino JC, Barboza CA, Vazquez PA, De Boni L, Atvars TD, et al. Excited-state and two-photon absorption in salicylidene molecules: the role of Zn (II) planarization. J Phys Chem C 2016;120(7):4032–9.
[13] Valiev RR, Fliegl H, Sundholm D. Insights into magnetically induced current pathways and optical properties of isophlorins. J Phys Chem A 2013;117 (37):9062–8.
[14] Benkyi I, Fliegl H, Valiev RR, Sundholm D. New insights into aromatic pathways of carbachlorins and carbaporphyrins based on calculations of magnetically induced current densities. Phys Chem Chem Phys 2016;18 (17):11932–41.
[15] Gershoni-Poranne R, Stanger A. Magnetic criteria of aromaticity. Chem Soc Rev 2015;44(18):6597–615.
[16] Heine T, Corminboeuf C, Seifert G. The magnetic shielding function of molecules and Pi-electron delocalization. Chem Rev 2005;105 (10):3889–910.
[17] Sulzer D, Olejniczak M, Bast R, Saue T. 4-Component relativistic magnetically induced current density using London atomic orbitals. Phys Chem Chem Phys 2011;13(46):20682–9.
[18] Storr T, Wasinger EC, Pratt RC, Stack TDP. The geometric and electronic structure of a one-electron-oxidized nickel (II) Bis (salicylidene) diamine Complex. Angew Chem 2007;119(27):5290–3.
[19] Perdew JP, Burke K, Ernzerhof M. Generalized gradient approximation made simple. Phys Rev Lett 1996;77(18):3865–8.
[20] Raghavachari K, Trucks GW. Highly correlated systems. excitation energies of first row transition metals Sc–Cu. J Chem Phys 1989;91(2):1062–5.
[21] Krishnan R, Binkley JS, Seeger R, Pople JA. Self-consistent molecular orbital methods. XX. A basis set for correlated wave functions. J Chem Phys 1980;72 (1):650–4.
[22] Frisch MJ, Trucks MJ, Schlegel HB, Scuseria GE, Robb MA, Cheeseman JR, et al. Gaussian 092009.
[23] Scalmani G, Frisch MJ, Mennucci B, Tomasi J, Cammi R, Barone V. Geometries and properties of excited states in the gas phase and in solution: theory and application of a time-dependent density functional theory polarizable continuum model. J Chem Phys 2006;124(9):094107.
[24] Mennucci B, Cappelli C, Guido CA, Cammi R, Tomasi J. Structures and properties of electronically excited chromophores in solution from the polarizable continuum model coupled to the time-dependent density functional theory. J Phys Chem A 2009;113(13):3009–20.
[25] Saue T, Enevoldsen T, Helgaker T, Jensen HA, Laerdahl J, Ruud K, et al. DIRAC, a relativistic ab initio electronic structure program. Release DIRAC10; 2000.
[26] Visscher L. Approximate molecular relativistic Dirac-Coulomb calculations using a simple Coulombic correction. Theor Chem Acc 1997;98(2):68–70.
[27] Iliaš M, Jensen HJA, Bast R, Saue T. Gauge origin independent calculations of molecular magnetisabilities in relativistic four-component theory. Mol Phys 2013;111(9–11):1373–81.
[28] Dunning TH. Gaussian basis sets for use in correlated molecular calculations. I. The atoms boron through neon and hydrogen. J Chem Phys 1989;90 (2):1007–23.
[29] Brown D, Brownrigg R, Haley M, Huang W. The NCAR Command Language (NCL) (version 6.0. 0). UCAR/NCAR Computational and Information Systems Laboratory, Boulder, CO; 2012 [Available online at https://doi.org/10.5065/D6WD3XH5].
[30] Adamo C, Barone V. Toward reliable density functional methods without adjustable parameters: the PBE0 Model. J Chem Phys 1999;110:6158.
[31] Zarei SA, Khaledian D, Akhtari K, Hassanzadeh K. Copper (II) and nickel (II) complexes of tetradentate Schiff base ligand: UV-Vis and FT-IR spectra and DFT calculation of electronic, vibrational and nonlinear optical properties. Mol Phys 2015;113(21):3296–302.
[32] Lecarme L, Chiang L, Philouze C, Jarjayes O, Storr T, Thomas F. Detailed geometric and electronic structures of a one-electron-oxidized Ni salophen complex and its amido derivatives. Eur J Inorg Chem 2014;2014 (22):3479–87.
[33] Arıcı C, Ercan F, Kurtaran R, Atakol O. [N,N′-Bis (salicylidene)-2, 2-dimethyl-1, 3-propanediaminato] nickel (II) and [N,N′-bis (salicylidene)-2, 2-dimethyl-1, 3-propanediaminato] copper (II). Acta Crystallogr Sect C: Cryst Struct Commun 2001;57(7):812–4.
[34] More M, Pawal S, Lolage S, Chavan S. Syntheses, structural characterization, luminescence and optical studies of Ni (II) and Zn (II) complexes containing salophen ligand. J Mol Struct 2017;1128:419–27.
[35] Germino JC, Barboza CA, Quites FJ, Vazquez PAM, Atvars TDZ. Dual emissions of Salicylidene-5-chloroaminepyridine Due to excited state intramolecular

proton transfer: dynamic photophysical and theoretical studies. J Phys Chem C 2015;119(49):27666–75.
[36] Bast R, Jusélius J, Saue T. 4-Component relativistic calculation of the magnetically induced current density in the group 15 heteroaromatic compounds. Chem Phys 2009;356(1):187–94.
[37] Jacquemin D, Mennucci B, Adamo C. Excited-state calculations with TD-DFT: from benchmarks to simulations in complex environments. Phys Chem Chem Phys 2011;13:16987–98.
[38] Cai ZL, Sendt K, Reimers JR. Failure of density-functional theory and time-dependent density-functional theory for large extended π systems. J Phys Chem 2002;117:5543–9.
[39] Grimme S, Parac M. Substantial errors from time-dependent density functional theory for the calculation of excited states of large π systems. ChemPhysChem 2003;3:292–5.
[40] Dreuw A, Flemming RG, Head-Gordon M. Charge-transfer state as a possible signature of a zeaxanthin−chlorophyll dimer in the non-photochemical quenching process in green plants. J Phys Chem B 2003;107:6500–3.
[41] Sobolewski AL, Domcke W. Ab initio study of the excited-state coupled electron–proton-transfer process in the 2-aminopyridine dimer. Chem Phys 2003;294:73–83.
[42] Dreuw A, Head-Gordon M. Failure of time-dependent density functional theory for long-range charge-transfer excited states: the zincbacteriochlorin-bacteriochlorin and bacteriochlorophyll-spheroidene complexes. JACS 2004;126:4007–16.
[43] Fliegl H, Pichierri F, Sundholm D. Antiaromatic character of 16 π electron octaethylporphyrins: magnetically induced ring currents from DFT-GIMIC calculations. J Phys Chem A 2014;119(11):2344–50.